

show variations of 3 dB. Taking into account this result, it appears that the waveguide interconnects are the main source of variation. However, the major uncertainty in the fabrication does not stem from the demanding mechanical tolerances, which have been met very precisely, but rather from the conductive bonding of the substrates to the carrier plate. This cannot be carried out with sufficient reproducibility and uniformity in the manual fabrication process employed. A significant improvement is expected when using stamped conductive-bonding film and a professional multi-layer press.

The conversion gain variations are compensated for by individual adjustment of digitally programmable attenuators in the IF circuitry. Additionally, a final correction of element gain and phase errors is applied in the digital circuitry.

5. CONCLUSION

A novel highly integrated 4×4 receiver array module for digital beamforming in the Ka-band has been designed and fabricated. It incorporates 16 antenna elements, together with individual analog heterodyne receiver circuits, all packaged in a compact module of $30 \times 30 \times 92 \text{ mm}^3$ size, thus allowing us to array several modules in order to form a complete terminal. The first measurement results from the fabricated prototype module prove the functionality of the packaging concept. Critical issues, for example, the fabrication of the waveguide interconnects, have been identified and will be the subject of further optimization.

ACKNOWLEDGMENTS

The authors wish to acknowledge the support of the project administration at the German Space Center (DLR), Bonn, and the funding of this work by the German Ministry of Education and Research (BMBF).

REFERENCES

1. L.C. Stange, H. Pawlak, A. Dreher, S. Holzwarth, A.F. Jacob, O. Litschke, and M. Thiel, Components of a highly integrated DBF terminal antenna for mobile Ka-band satellite communications, *IEEE MTT-S Int Microwave Symp Dig 1* (2003), 583–586.
2. A. Dreher, D. Heberling, S. Holzwarth, C. Hunscher, A.F. Jacob, N. Niklasch, H. Pawlak, L. Richard, A. Schroth, L.C. Stange, and M. Thiel, Ka-band DBF terminal concepts for broadband satellite communications, *25th ESA Antenna Wkshp Satellite Antenna Technol*, Noordwijk, The Netherlands, 2002, pp. 95–102.
3. M.S. Hauhe and J.J. Wooldridge, High density packaging of X-band active array modules, *IEEE Trans Comp Packag Technol B* 20 (1997), 279–291.

© 2004 Wiley Periodicals, Inc.

SPATIAL DOMAIN GREEN'S FUNCTIONS FOR PLANAR MULTILAYERED STRUCTURES

K. L. Lai,¹ L. Tsang,^{1,2} and C. C. Huang²

¹ Wireless Communications Research Center
City University of Hong Kong

Hong Kong, SAR

² Electrical Engineering Department

University of Washington

Box 352500

Seattle, WA 98195-2500

Received 28 May 2004

ABSTRACT: This paper presents a robust approach for calculating spatial-domain Green's functions on the interface or close to the interface of planar multilayered microstrip structures with lossless or lossy dielectric materials for a wide range of frequencies and layer thicknesses. We compute the mixed potential Green's functions for distance ρ for 200 points from 0.1 to 10 wavelengths. The CPU is less than 30 s for each frequency on a Pentium-IV 2.4-GHz PC. In the case of moderate layer thickness, the fast Fourier transform (FFT) method is introduced to the half-space extraction method in order to calculate all ρ values of the different radial source-to-field separations simultaneously. For thin layers, the results are computed by the contributions of the vertical-branch cut and the addition of a surface-wave pole. © 2004 Wiley Periodicals, Inc. *Microwave Opt Technol Lett* 44: 86–91, 2005; Published online in Wiley InterScience (www.interscience.wiley.com). DOI 10.1002/mop.20555

Key words: spatial-domain Green's function; fast Fourier transform (FFT); vertical-branch cut; surface wave poles; leaky-wave poles

1. INTRODUCTION

Computation of electric-field Green's functions for multilayered media is always a critical concern for the formulations of integral equations in many electromagnetic problems. Green's functions of single-layered media have been studied using the complex-image method [1, 2]. Another approach is based on the representation of the spectral-domain Green's function in terms of a pole-residue form [3, 4]. Time-domain layered-media Green's functions have also been evaluated [5]. For problems of interconnects in printed circuit boards, the frequencies usually range from 500 MHz to 20 GHz, whereas the distances range from 0.01 to 10 free-space wavelengths. There are also varying dielectric thicknesses of multilayered media. A fast and robust method is required to evaluate the layered-medium Green's functions with the following requirements: (a) a multilayered medium, (b) lossless and lossy dielectrics, (c) a wide range of frequencies corresponding to wide range of thicknesses, and (d) distances ρ a range of 0.01 to 10 free-space wavelengths. To cover these wide ranges of variations, in this paper we present two complementary methods to cover all these requirements for the mixed-potential Green's functions. The first method is to solve problems of moderate thickness of d (total thickness), with $d > 0.05\lambda_0$. The spatial-domain Green's functions are calculated using fast Fourier transform (FFT) method, based on the half-space extraction method [6, 7]. The computation time for simultaneously evaluating the Green's functions of 200 different source-to-field distances, ranging from 0.01 to 10 free-space wavelengths for each frequency, consumes about 20 s. The second method is applied for total thickness with $0 < d \leq 0.05\lambda_0$, using the numerical integration along the vertical-branch cut together with the surface-wave pole extraction. The time of calculating 200 different values of ρ , ranging from 0.01 to 10

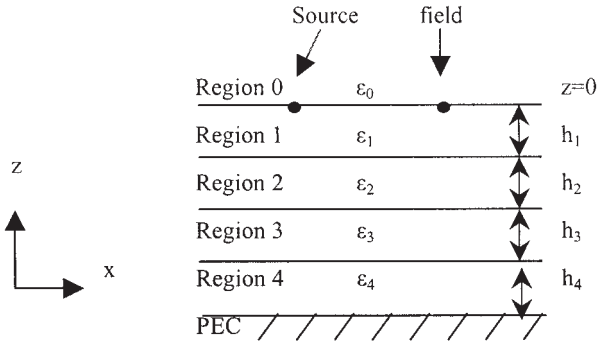


Figure 1 Side view of a four-layered medium with a dielectric substrate above a ground plane

free-space wavelengths, requires about 30 s for each frequency. The surface-wave poles are extracted by means of the Newton–Raphson method [8], which can be easily implemented for multi-layered media. There are no contributions from the leaky-wave poles for d of less than 0.05 wavelengths when the vertical-branch cut is chosen as the path of integration. In this paper, we present the numerical results for a four-layered medium with two thicknesses. One is moderate thickness, with d equal to $0.2\lambda_0$, where the Green’s function is calculated by the FFT based on half-space extraction. Another thickness of $0.02\lambda_0$ is adopted for the vertical-branch-cut integration approach, and 200 different values of ρ are chosen from 0.01 to 10 free-space wavelengths. For wave-propagation problems, the formulations of impedance-matrix elements via the method of moments (MoM) requires a robust Green’s function calculation approach for a wide range of frequencies and dielectric thicknesses. The approach presented in this paper has been fully implemented in the problems of interconnects for filling the impedance-matrix elements [9].

2. FAST FOURIER TRANSFORM VIA HALF-SPACE EXTRACTION FOR $d > 0.05\lambda_0$

In this section, the FFT is applied based on the half-space extraction method [6, 7] for Green’s function solutions. Figure 1 shows a four-layered medium structure with various dielectric materials and thicknesses above a perfect electric conductor (PEC). Region 0 is defined as air. Some of the dielectric materials are lossless and some are lossy. The electric-field spatial-domain Green’s functions for mixed potentials, G_A and G_V , with source and field points on the surface of the dielectric substrates are expressed by

$$G_A(\rho) = -\frac{j\mu_0}{4\pi} \int_0^\infty dk_\rho \frac{k_\rho}{k_z} J_0(k_\rho \rho) (e^{-jk|z-z'|} + R^{TE} e^{-jk(z+z')}), \quad (1a)$$

$$G_V(\rho) = -\frac{j}{4\pi\epsilon_0} \int_0^\infty dk_\rho \frac{k_\rho}{k_z} J_0(k_\rho \rho) \times \left(e^{-jk|z-z'|} + \frac{k^2 R^{TE} + k_z^2 R^{TM}}{k_\rho^2} e^{-jk(z+z')} \right), \quad (1b)$$

where $k = 2\pi/\lambda_0$, $k_\rho = \sqrt{k_x^2 + k_y^2}$, $k_z = \sqrt{k^2 - k_\rho^2}$, ρ is the source-to-field distance on the x - y plane, and z and z' are the vertical positions of the horizontal source and observation points, respectively. The electric field at the field point is observed horizontally. For surface-field evaluation, $z = z' = 0$. R^{TE} and R^{TM} are the reflection coefficients for the transverse electric (TE) and

transverse magnetic (TM) waves, respectively, whose formulations are shown in [10]. $J_0(k_\rho \rho)$ is the Bessel function of 0th order. In [7], the integration is carried out on the Sommerfeld integration path with half-space extraction due to singularities on the real k_ρ axis. For the following, only formulations of scalar potential G_V are presented.

To calculate for surface-field solutions with different values of ρ simultaneously, the numerical integrals of the half-space extracted part are integrated by means of the FFT method in [11]. Firstly, Eq. (1) is separated into three parts. The first part corresponds to free-space solutions, and is analytically solved by the Sommerfeld identity [12] (Figure 2). The second part corresponds to the half-space case, and the third part refers to a layered medium with half-space extraction, given by

$$G_V^{(N)}(\rho) = \int_0^\infty dk_\rho g_V(k_\rho) J_0(k_\rho \rho) \exp(-\nu_R k_\rho), \quad (2)$$

where

$$g_V(k_\rho) = -\frac{j}{4\pi\epsilon_0} \frac{1}{k_z k_\rho} [k^2(R^{TE} - R_{01}^{TE}) + k_z^2(R^{TM} - R_{01}^{TM})] \exp(\nu_R k_\rho). \quad (3)$$

By applying the FFT, the identity in [13] is used as follows:

$$\int_0^\infty dk_\rho J_n(k_\rho \rho) \exp(-\nu k_\rho) = \frac{(\sqrt{\nu^2 + \rho^2} - \nu)^n}{\rho^n \sqrt{\nu^2 + \rho^2}}, \quad n > -1; \nu = \nu_R + i\nu_I. \quad (4)$$

We rewrite Eq. (4) in terms of the FFT formulations as follows:

$$g(k_\rho) = \frac{1}{N\Delta k_\rho} \sum_{n=-N/2}^{(N/2)-1} a(f) \exp(-j2\pi f k_\rho), \quad 0 < k_\rho < \left(\frac{N}{2} - 1\right) \Delta k_\rho, \quad (5)$$

where

$$a(f) = \int_{-\infty}^\infty dk_\rho g(k_\rho) \exp(-j2\pi f k_\rho), \quad f = \frac{n}{N\Delta k_\rho}. \quad (6)$$

In [11], for the proper choice of N , the number of samples should be in some integral power of 2. The right-hand side of Eq. (5) is periodic and does not tend towards zero at ∞ ; thus, we multiply Eq. (5) by $\exp(-\nu_R k_\rho)$. Then, we alias the functions $g_V(k_\rho)$ into periodic sequences $g_V^p(k_\rho)$ and the periodic subroutines are expressed as

$$a_V^p\left(\frac{n}{N\Delta k_\rho}\right) = \Delta k_\rho \sum_{\ell=0}^{N-1} g_V^p(\ell\Delta k_\rho) e^{-j2\pi\ell n/N}; \quad n = 0, 1, \dots, N-1. \quad (7)$$

The final solution then becomes

$$G_V^N(\rho) = \frac{1}{N\Delta k_\rho} \sum_{n=0}^{N-1} a_V\left(\frac{n}{N\Delta k_\rho}\right) \frac{1}{\sqrt{\nu^2 + \rho^2}}, \quad (8)$$

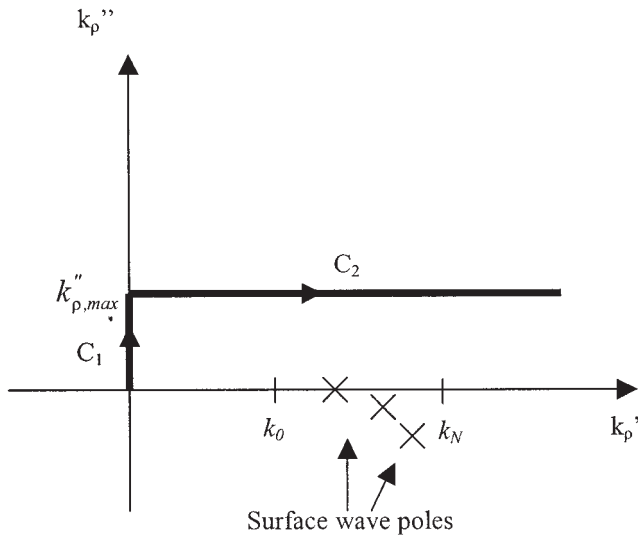


Figure 2 Sommerfeld contour integration path used in numerical integration of the half-space extraction $C_1 + C_2$

where the aperiodic sequence $a_v(n/N\Delta k_\rho)$ is firstly de-aliased from the outcome of Eq. (7) for G_V . It is noted that the integration path of original formulation of FFT in Eq. (5) is along the real axis. Because singularities may occur on the real k_ρ axis, we need to take the integration sequence $g_v(k_\rho)$ above the real k_ρ axis. In the integration, we take $k_\rho = k'_\rho + jk''_\rho$, where $k''_{\rho, \max} = 1/d$, $k'_{\rho, \max} = \max(15/d, 10 \operatorname{Re}(k_N))$ and $\Delta k_\rho = 2k'_{\rho, \max}/N_T$, where k_N refers to the wave number associated with the N^{th} -layer substrate, $N_T = 20,000$ sample points, and $v_R = d/8$.

3. FORMULATIONS OF VERTICAL-BRANCH CUT AND SURFACE-WAVE POLES FOR $0 < d \leq 0.05\lambda_0$

For a thin-layered medium, the performance of the half-space extraction method degrades. The integration is carried out on the vertical-branch cut associated with k_0 (BC0), as shown in Figure 3. When the vertical-branch cut is chosen as the path of integration, the contribution of the leaky-wave poles are out of consideration in the Green's function calculation within this range of d . The inte-

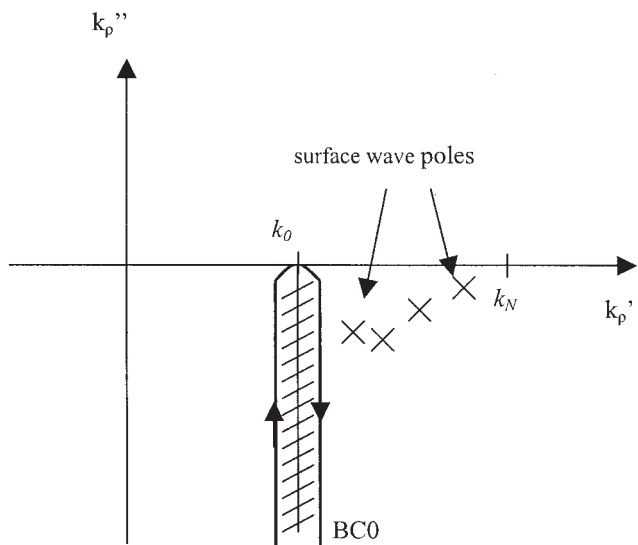


Figure 3 Integration path of branch cut for numerical vertical-branch-cut integration and possible surface-wave pole locations for layered media

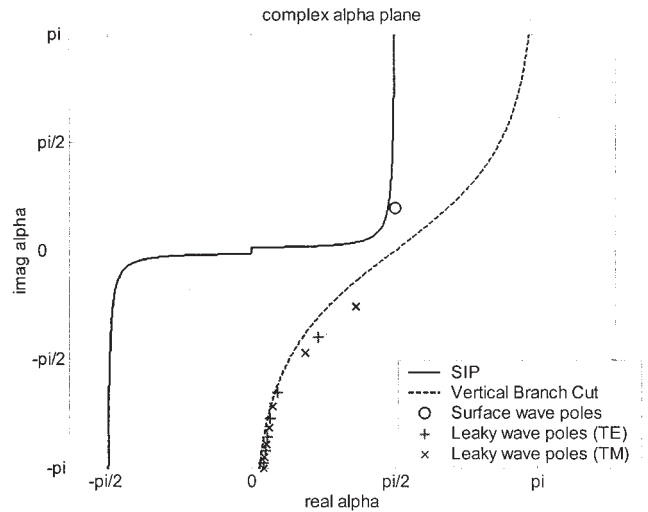


Figure 4 Approximate locations of surface-wave poles and leaky-wave poles on the complex α plane and the corresponding vertical-branch-cut integration path and the SIP of a single-layered medium of thickness $0.01\lambda_0$ and permittivity 4

grand decays exponentially along the vertical-branch cut due to the presence of the term of the Hankel function. The expressions for G_V is given by

$$G_V(\rho) = -\frac{j}{8\pi\epsilon_0} \int_{VBC} dk_\rho \frac{1}{k_z} \left[k_\rho + \frac{k^2 R^{TE} + k_z^2 R^{TM}}{k_\rho} \right] H_0^{(2)}(k_\rho \rho). \quad (9)$$

In Eq. (9), the integration is carried out along the path $k_\rho = k_0 + jk''_\rho$, where k''_ρ goes from $-\infty$ to 0. On the vertical branch cut associated with k_0 , $(k_z)_R$ is defined as k_z on the right side of the vertical-branch cut, with $(k_z)_L$ as that on the left, $(k_z)_L = -(k_z)_R$, and $k_{e_z} = \sqrt{k_\ell^2 - k_\rho^2}$. Multilayered dielectric substrates with any other materials can also be applied using this approach. By means of Cauchy's integral theorem, the vertical-branch-cut integration associated with k_0 and the surface-wave and leaky-wave pole extractions need to be included in the resultant solutions. We consider single-layered material with relative permittivity ϵ_r located onto the PEC. In the analysis, by means of the complex α plane, we set $k_\rho = k_0 \sin \alpha$. In Figure 4, we stretch the approximate locations of surface-wave poles and leaky-wave poles on the complex α plane, the vertical-branch-cut integration path, and the SIP described. For extractions of the surface-wave and leaky-wave poles, we adopt the Newton-Raphson method [8]. The surface-wave and leaky-wave poles are found based on the characteristic equations. Since the surface-wave poles are located between $\operatorname{Re}(k_0)$ to $\operatorname{Re}(k_N)$ on the 4th quadrant of the complex k_ρ plane, where k_N is the wave number of region N in the N -layered medium structure, the initial searching points of the Newton method are on the real k_ρ axis, starting from $\operatorname{Re}(k)$ to $\operatorname{Re}(k_N)$. The locations of the leaky-wave poles are on the bottom Riemann sheet, while that of the surface-wave poles are located on the upper Riemann sheet. The solutions of the surface-wave and leaky-wave poles are obtained from different characteristic equations [10]. An infinite number of leaky-wave poles exist. However, when d is less than $0.05\lambda_0$, the leaky-wave pole extractions are located on the right-hand side of the vertical-branch cut, as shown in Figure 4. By Cauchy's integral theorem, the leaky-wave pole does not contribute to the Green's function determination, for this range of d . The fact that leaky-wave poles do not contribute is a result of using the

vertical-branch cut as the integration path. For evaluation of mixed potentials with thin-layered substrates, only surface-wave pole extraction has to be applied, together with the vertical-branch-cut integration. The analytic expression of the surface-wave pole contribution of the TE poles is given by

$$G_{v,sw}^{TE}(\rho) = -\frac{j}{8\pi\epsilon_0} \frac{k^2}{k_{pp}} H_0^{(2)}(k_\rho \rho) res^{TE}, \quad (10)$$

where res^{TE} is the residues of R^{TE} . The TM poles are formulated in a similar manner. The analytic expression for the residue is given by

$$res^{TE} = \sum_{p(TE)} \frac{1}{k_z} \left|_{k_\rho=k_{pp}, k_p \rightarrow k_{pp}} \lim (k_p - k_{pp}) R^{TE}. \quad (11)$$

Thus, we solve G_V in Eq. (9) for the vertical-branch-cut integration, and Eq. (10) for the surface-wave pole extraction for thin-layered media. Since the integrand decays exponentially along the vertical-branch-cut integration due to the Hankel function, the number of integration samples can be greatly reduced to achieve accurate results. In the integration, we use $k_{\rho, \max}'' = 10/\rho_{\max}$ and Δk_ρ is separated via logarithmic scale into about 20,000 integration points. A frequency of 1 GHz is used.

4. IMPEDANCE-MATRIX ELEMENTS

In [9], the interconnect problem has 150 unknowns; thus, we solve for thousands of unknowns of the impedance-matrix elements. However, thousands of unknowns are usually adopted in an interconnect problem, and a high number of computations of the Green's function is required. Based on the robust Green's function evaluation methods, this was fully implemented in [9]. A formulation of the impedance-matrix elements using the present approach with a distance range from 0.01 to $3\lambda_0$ and a frequency range from 500 MHz to 20 GHz has been implemented. This section demonstrates how this approach can be applied to formulate the impedance-matrix elements. The formulation of the impedance-matrix elements for nonoverlapped patches is given by

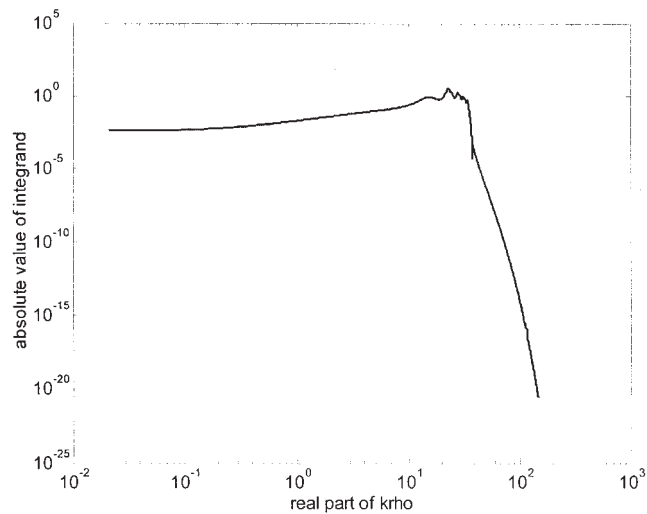


Figure 5 Absolute value of the integrand in Eq. (1) with half-space extraction. A log-log scale is used, showing the exponential decay for large k_ρ (integrands are on the C_2 of the Sommerfeld integration path with $k_{\rho, \max}'' = 3.353$; $\rho = 0.1\lambda_0 = 0.03$ m)

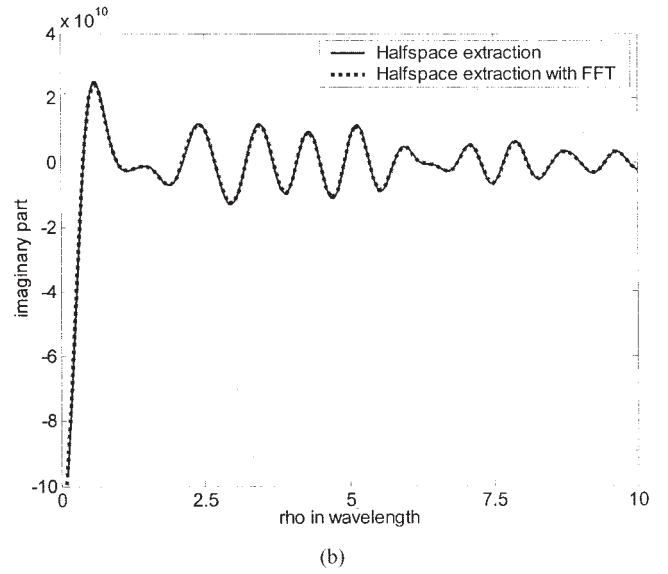
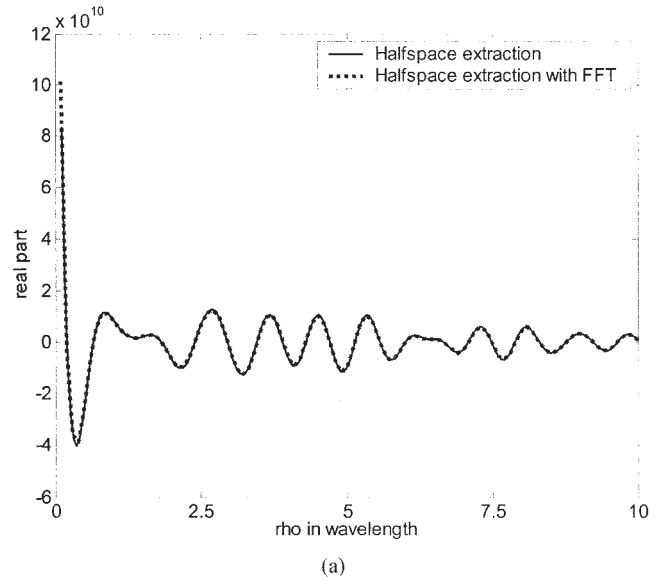


Figure 6 Real and imaginary parts of the surface electric fields of the spatial Green's functions as a function of distance r in a range of 0.01 to $10\lambda_0$ with parameters: frequency = 1 GHz, $\epsilon_1 = 3\epsilon_0$, $\epsilon_2 = (3.1 - j0.1)\epsilon_0$, $\epsilon_3 = (3.2 - j0.05)\epsilon_0$, and $\epsilon_4 = 3.3\epsilon_0$; thicknesses: 0.015, 0.012, 0.018, and 0.015 m, respectively

$$Z_{mm} = j\omega\mu_0 \cdot A_m A_n \cdot \bar{T}_m^{+/-}(\bar{r}_{mc}) \cdot \bar{G}_A(\bar{r}_{mc}, \bar{r}_{nc}) \cdot \bar{T}_n^{+/-}(\bar{r}_{nc}) - \frac{j}{\omega\epsilon_0} \cdot A_m A_n \nabla_S \cdot \bar{T}_m^{+/-}(\bar{r}_{mc}) \cdot G_V(\bar{r}_{mc}, \bar{r}_{nc}) \cdot \nabla_S' \cdot \bar{T}_n^{+/-}(\bar{r}_{nc}). \quad (12)$$

Note that the impedance-matrix element formulation is a function of mixed potentials \bar{G}_A and G_V .

5. RESULTS AND DISCUSSION

We first demonstrate the numerical results using the FFT approach based on the half-space extraction method. For a layered medium configuration (as in Fig. 1), where region 0 is air, region 1 has $\epsilon_1 = 3\epsilon_0$, region 2 has $\epsilon_2 = (3.1 - j0.1)\epsilon_0$, region 3 has $\epsilon_3 = (3.2 - j0.05)\epsilon_0$, and region 4 has $\epsilon_4 = 3.3\epsilon_0$. The bottom layer refers to the perfect electric conductor (PEC) layer. The operating frequency is 1 GHz and the dielectric thicknesses of each layer of

regions 1–4 are 0.015, 0.012, 0.018, and 0.015 m, respectively. In Figure 5, we show the numerical integrand of G_V with half-space extraction along the Sommerfeld integration path. We plot the magnitude of the integrand along the C_2 of the SIP as a function with increasing k'_ρ on a log-log scale. As we can see, the integrand decays exponentially as the value of k'_ρ increases. Since the integration path C_2 is above the real k_ρ axis, the denominators of R^{TE} and R^{TM} are never equal to zero. The peak of the integrand occurs when the path is closest to the surface-wave poles.

Due to the large variations in magnitude for ρ , ranging from 0.01 to 10 free-space wavelengths in Green's function solutions, we plot the numerical results for the real and imaginary parts of G_V . Figure 6 shows the real and imaginary parts of the calculated mixed potential G_V as a function of source-to-field distance from 0.01 to 10 free-space wavelengths using the above configuration. With this configuration, half-space extraction via FFT method is used. The numerical outcome using the half-space extraction method without FFT is also shown in the figure. We can see that solutions match in both real and imaginary parts for the specified range of ρ and the results remain unchanged whenever the FFT is applied. This reveals that the computational time of the evaluation of mixed potential G_V is about 20 s for 200 different values of ρ using the FFT method based on half-space extraction, while that without FFT requires more than 5 min. The simulations are carried on a PC with a 2.4-GHz CPU.

For moderate thickness of d , the fast Fourier transform method with half-space extraction is applied. The introduction of the FFT method [11] leads to a reduction in computation time by evaluating all ρ simultaneously for each frequency. However, the performance of the half-space extraction method degrades when the dielectric thickness decreases. It is found that solutions of large percentage errors occur with the use of this extraction method for small thickness of d , which results in the introduction of another complementary method for evaluating the spatial-domain Green's function with a dielectric of thin multi-layered media. Numerical integration along the vertical-branch cut is implemented instead of the Sommerfeld integration path. The integrand oscillates less by means of the Hankel function. With the addition of surface-wave

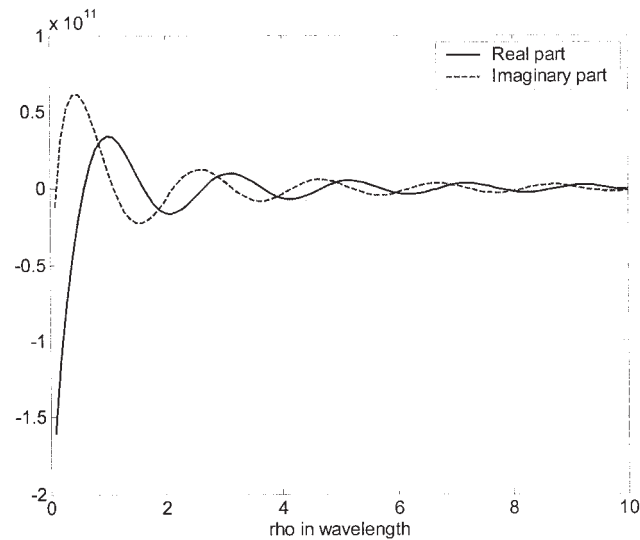


Figure 7 Real and imaginary parts of the surface electric fields of the spatial Green's functions as a function of distance ρ in a range of 0.01 to $10\lambda_0$ using the vertical-branch-cut approach with parameters: frequency = 1 GHz, $\epsilon_1 = 3\epsilon_0$, $\epsilon_2 = (3.1 - j0.1)\epsilon_0$, $\epsilon_3 = (3.2 - j0.05)\epsilon_0$, and $\epsilon_4 = 3.3\epsilon_0$; thicknesses for each layer: 1.5, 1.2, 1.8, and 1.5 mm, respectively

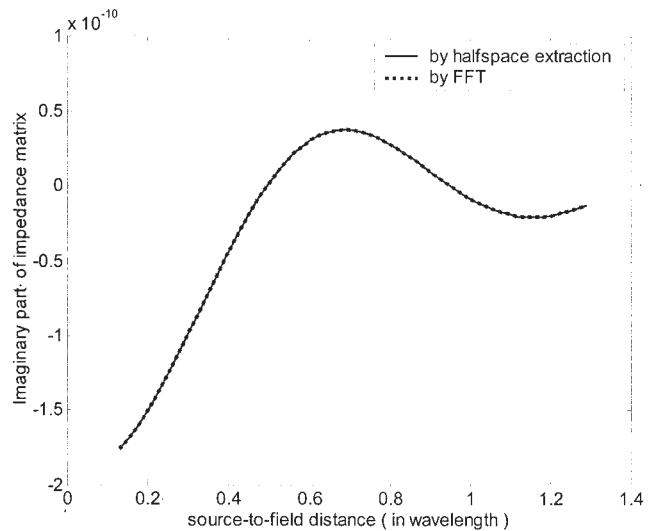
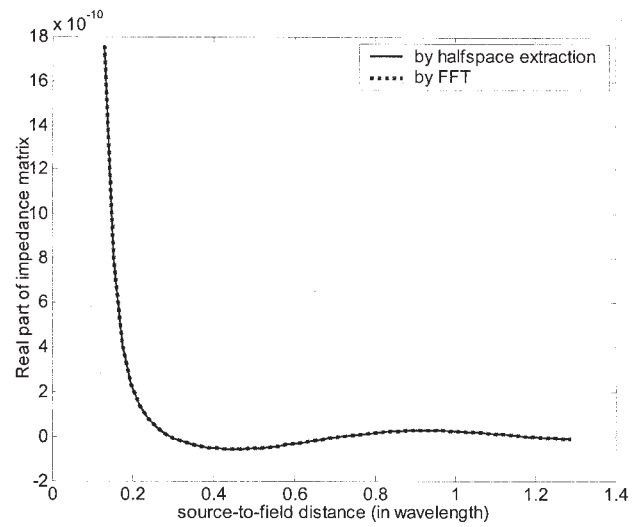


Figure 8 (a) Real and (b) imaginary parts of the impedance-matrix elements as a function of the distance between the m^{th} patch and the n^{th} patch (vertical-branch-cut integration with surface-wave-pole extraction is used)

and leaky-wave pole extractions, accurate solutions can be obtained. In Figure 7, we use the above layered medium with the same dielectric materials, but different thicknesses. The thicknesses for each region (regions 1–4) are 1.5, 1.2, 1.8, and 1.5 mm, respectively. Thus, the total thickness of the layered medium becomes $0.02\lambda_0$ at a frequency of 1 GHz. The numerical results for the real and imaginary parts of G_V are shown, respectively, revealing that there are no leaky-wave poles when $0 < d \leq 0.05\lambda_0$, and hence the difficult-to-locate leaky-wave poles do not need to be extracted. It is demonstrated that the computational time of the mixed potential calculations is about 30 s using the vertical-branch-cut integration for the 200 different source-to-field separations.

This approach has been found to be especially efficient in the analysis of via discontinuity when generating impedance-matrix elements by the method of moments (MoM), which requires a high number of Green's function solutions to be calculated. It has been implemented in interconnect problems [9]. To verify the accuracy, we verify the numerical outcome using the formulation in Eq. (12). In this case, the layered medium contains one layer with dielectric

constant of 4.001 and thickness of 0.254 mm, that is, 10 mil. The working frequency is 8.09 GHz; hence, the thickness is $0.00685\lambda_0$. The solutions of the mixed potentials G_A and G_V have been calculated using the vertical-branch-cut integration with surface-wave pole extraction. Figure 8 shows the magnitude of the impedance-matrix elements Z_{mn} with the m^{th} patch centered at (x_m, y_m) and n^{th} patch centered at (x_n, y_n) . The result using the vertical-branch-cut approach is compared with that using the higher-order asymptotic method [6]. The results show that both methods result in the same output, as shown in Figure 8.

ACKNOWLEDGMENT

This work is supported by Hong Kong Research Grant Council, Hong Kong SAR, China, under CityU grant no. 9380034.

REFERENCES

1. Y.L. Chow, J.J. Yang, D.G. Fang, and G.E. Howard, A closed-form spatial green's function for the thick microstrip substrate, *IEEE Trans Microwave Theory Tech* 39 (1991).
2. R.A. Kipp and C.H. Chan, Complex image method for sources in bounded regions of multilayer structures, *IEEE Trans Microwave Theory Tech* 42 (1994).
3. V.I. Okhmatovski and A.C. Cangellaris, A new technique for the derivation of closed-form electromagnetic Green's functions for unbounded planar layered media, *IEEE Trans Antennas Propagat* 50 (2002).
4. V.I. Okhmatovski and A.C. Cangellaris, Evaluation of layered media Green's functions via rational function fitting, *IEEE Microwave Wireless Compon Lett* 14 (2004).
5. L. Tsang, C.-J. Ong, C.-C. Huang, and V. Jandhyala, Evaluation of the Green's function for the mixed potential integral equation (MPIE) method in the time domain for layered media, *IEEE Trans Antennas Propagat* 51 (2003), 1559–1571.
6. L. Tsang, J.-H. Cha, and J.R. Thomas, Electric fields of spatial Green's functions of microstrip structures and applications to the calculations of impedance matrix elements, *Microwave Opt Technol Lett* 20 (1999), 90–97.
7. L. Tsang, C.C. Huang, and C.H. Chan, Surface electric fields and spatial derivatives of Green's function of layered media based on half-space extraction, *Microwave Opt Technol Lett* 24 (2000), 247–253.
8. T. Nakata, N. Takahashi, K. Fujiwara, N. Okamoto, and K. Muramatsu, Improvements of convergence characteristics of Newton–Raphson method for nonlinear magnetic-field analysis, *IEEE Trans Magn* 28 (1992).
9. C.C. Huang and L. Tsang, Analysis of via discontinuity on the printed circuit board (PCB), (to appear).
10. W.C. Chew, *Fields and waves in inhomogeneous media*, IEEE Press, New York, 1995, p. 49.
11. L. Tsang, R. Brown, J.A. Kong, and G. Simmons, Numerical evaluation of electromagnetic fields due to dipole antennas in the presence of stratified media, *J Geophysical Res* 79 (1974).
12. J.A. Kong, *Electromagnetic wave theory*, Wiley–Interscience, New York, 1990.
13. I.S. Gradshteyn and I.M. Ryzhik, *Table of integrals, series, and products*, Academic Press, London.

© 2004 Wiley Periodicals, Inc.

AN UNTILTED EDGE-SLOTTED WAVEGUIDE ANTENNA ARRAY WITH VERY LOW CROSS-POLARIZATION

Wei Wang, Shun-Shi Zhong, Jian Jin, and Xian-Ling Liang
School of Communication and Information Engineering
Shanghai University
Shanghai 200072, P.R. China

Received 4 June 2004

ABSTRACT: A novel untilted edge-slotted waveguide antenna array with very low cross-polarization is presented, in which the radiating element is composed of an untilted narrow-wall slot and a pair of shaped irises that flank the slot in the waveguide. An array with 16 proposed elements for X-band application is designed and measured. The experimental results show that the antenna has an excellent cross-polarization level of < -40 dB and over 7% bandwidth of $VSWR \leq 1.5$. © 2004 Wiley Periodicals, Inc. *Microwave Opt Technol Lett* 44: 91–93, 2005; Published online in Wiley InterScience (www.interscience.wiley.com). DOI 10.1002/mop.20556

Key words: waveguide; slot; antenna

1. INTRODUCTION

The slotted waveguide antenna array has been used in radar and communication systems widely due to its easy fabrication, agile aperture-distribution control, and low loss. In this antenna, the radiating element is simply a narrow slot milled in the broad wall or the edge of a rectangular waveguide [1]. Normally, the edge slot must be inclined in order to be excited. However, the slot inclination produces an undesired component of the electric field orthogonal to the waveguide's longitudinal axis. This causes not only unwanted polarization, but also heightened back radiation. For the purpose of minimizing the presence of undesired cross polarization, some array approaches have been used [2], resulting in complex structures. Fortunately, a radiating element consisting of an untilted narrow wall slot and a pair of excitation wires was invented by Ajioka [3] and analyzed by Hashemi-Yeganeh et al. [4]. Furthermore, an untilted slot excited by a dielectric plate with conducting strips on both sides was developed [5]. Since the tilted holes for the wires must be drilled to the waveguide walls and then the tilted wires must be soldered to the walls, these untilted slots excited by tilted wires have problems with regard to the fabrication of a large array. Although the untilted slots excited by a dielectric plate with etched conducting strips can control the coupling more easily and more accurately than wire excitation, there is a problem that the dielectric plate must be fixed to the waveguide walls in a stable manner, especially for antennas working under difficult conditions.

In this paper, a new technique to excite the untilted slot in a narrow wall is proposed and an antenna array with very low cross-polarization composed of untilted slots is designed. Using a pair of shaped irises that flank the slot instead of the abovementioned wires or stripes, as shown in Figure 1(a), untilted slot-antenna excitation is realized. The proposed slot array can be fabricated more easily, especially as the slotted-waveguide antenna needs to be fabricated of carbon-fibre reinforced plastics (CFRP) for low mass, high stiffness, and perfect thermal stability in airborne and spaceborne applications. Based on the simulation carried out using the commercial software Ansoft HFSS, an antenna array for X-band applications is designed, fabricated, and measured. Then experimental results are presented to verify the design.